Chemical Engineering Journal Advances 26 (2026) 101111

Contents lists available at ScienceDirect

Chemical Engineering Journal Advances

journal homepage: www.sciencedirect.com/journal/chemical-engineering-journal-advances

Durable copper nanowires for flexible curvature sensors

Linda Broere [a,†], Rituporn Gogoi [a,†,*], Amit Barua [a], Nidhin George Mathews [c,‡], Sari Granroth [b], Kristofer Kolpakov [a], Gaurav Mohanty [c], Emilia Peltola [a], Vipul Sharma [a,*]

[a] Department of Mechanical and Materials Engineering, Faculty of Technology, University of Turku, Vesilinnantie 5 - 20500, Turku, Finland
[b] Department of Physics and Astronomy, Faculty of Science, University of Turku, Vesilinnantie 5 - 20500, Turku, Finland
[c] Materials science and Environmental Engineering, Faculty of Engineering and Natural Sciences, Tampere University, Korkeakoulunkatu 6 - 33014, Tampere, Finland

ARTICLE INFO

Keywords:
Robust nanowires
Temperature effect
Flexible electronics
Curvature sensor
Durable sensors

ABSTRACT

Metal nanowire-based flexible conducting surfaces (FCS) are vital for next-generation flexible and wearable sensors. Copper nanowires (CuNWs) offer a low-cost alternative to the expensive silver nanowires for fabricating FCS, yet their poor stability remains a significant challenge. In this study, we report the synthesis of ultralong CuNWs using a hydrothermal polyol method across a range of temperatures (120–180 °C). The CuNWs synthesised at 160 °C (CuNW-160) demonstrated the best performance. CuNW-160 films maintained stable conductivity for over 60 days in ambient conditions and thermal stability up to 140 °C. A capacitive curvature sensor was fabricated using FCS made with CuNW-160, which maintained consistent performance over 10,000 bending cycles and still showed good curvature sensitivity after 75 days. This highlights the potential use of the copper nanowires by tuning reaction temperature for use in reliable, low-cost flexible electronics.

Introduction

The growing demand for advanced human-machine interfaces in sensing [1], the Internet of Things [2], and healthcare monitoring [3] is driving the need for reliable electronic sensors. These devices convert mechanical stimuli such as touch, stretch, or bending into electrical signals for responsive machine interaction [4]. With the rise of flexible electronics, there is increasing importance placed on flexible and wearable touch sensors that can continuously monitor health and detect motion from mechanical deformation [5]. Such sensors commonly rely on deformable and surface conforming flexible conducting surfaces (FCS) [6].

Metal nanowires (MNWs) are promising materials owing to their high electrical conductivity and mechanical properties [7]. Crisscrossed MNW networks can be readily assembled onto elastomeric substrates to produce high-performance FCS for emerging electronics. Among MNWs, silver nanowires (AgNWs) are the state-of-the-art for electrical conductivity, but their high cost limits large-scale deployment [8]. Copper nanowires (CuNWs) offer comparable conductivity, but, as copper is ~1000 times more abundant and ~91 % less expensive than silver, CuNWs provide a cost-effective alternative [9]. Nevertheless, several challenges hinder CuNW commercialisation in flexible electronics, such as the difficulty of integration onto surfaces due to rapid aggregation on surfaces, unscalable synthesis methods and critically, short-term chemical stability [9]. Solutions include methods for elimination of nanoparticle by-products [10,11], synthesis methods that allow rapid reproducible growth [12], strategies for improved dispersibility [13] and synthetic strategies for ultra-long wires with superior percolation [14]. Both, silver and copper suffer from stability via rapid sulfidation [15] and oxidation issues [16,17] respectively, limiting their potential for practical usage. The stability of copper nanowires typically ranges from multiple hours [18] to several weeks [19]. Consequently, most systems require additional passivation strategies, either by individually coating the nanowires with protective materials [18] or by stabilising them within nanowire networks using polymeric encapsulants [20,21] to prevent oxidation. Although strategies such as storage in reducing environments and protective coatings can mitigate oxidation [22], stability remains a persistent bottleneck, and coatings add cost that significantly weakens copper's economic advantage [23].

In this study, we demonstrate that fine-tuning the reaction temperature produces copper nanowires with significantly enhanced intrinsic stability. We systematically investigated the influence of reaction

* Corresponding authors.
E-mail addresses: rigogo@utu.fi (R. Gogoi), vipul.sharma@utu.fi (V. Sharma).
† These authors contributed equally to the work.
‡ Current address: Advanced materials for nuclear energy, VTT Technical Research Centre of Finland, Espoo 02150, Finland.

https://doi.org/10.1016/j.ceja.2026.101111

Available online 24 February 2026

temperature on CuNW morphology and their corresponding stability under various environmental conditions. CuNWs synthesised at 160 °C retained stable electrical conductivity for more than 60 days, effectively doubling the lifetime (~30 days) typically achieved using existing method [24] and surpassing many coating-based stabilisation strategies reported to date [25,26]. These nanowires also exhibited improved thermal stability up to 140 °C and enhanced resilience under electrical loading. Device-level robustness was validated by integrating the CuNWs into flexible capacitive curvature sensors, which maintained consistent performance over 10,000 bending cycles. Collectively, this work advances the development of durable, high-performance CuNW--based flexible conductive surfaces and establishes temperature-guided synthesis as a cost-effective, scalable, one-pot route toward sustainable next-generation flexible electronics. To the best of our knowledge, this is the first systematic study directly linking synthesis temperature to both microstructural evolution and long-term device-level stability of CuNWs on flexible substrates.

Experimental

Materials and reagents

Copper (II) chloride dihydrate ($CuCl_2.2H_2O$, ACS reagent), oleylamine (OLA, C-18 content ~80–90 %), D-(+)-glucose and glycerol (≥99 %, analytical reagent grade) were purchased from Fisher Scientific. Oleic acid (OA, technical grade 90 %), propionic acid (≥99.5 %, ACS reagent), and n-hexane (≥99 %, laboratory reagent grade), formic acid (for synthesis, 98 %) and nylon-6 (N-6) pellets were purchased from Merck (Sigma-Aldrich). Ethanol was purchased from Altia Oy, and reverse osmosis water was obtained from a Puro™ reverse osmosis water purifier from Avidity Science. Polycarbonate (PC) substrate (0.1 μm pores, 47 mm diameter) was ordered from Pieper Filter GmbH.

Synthesis and fabrication

Synthesis of copper nanowires

CuNWs were synthesised based on a previously reported method [24] with some modifications. Typically, a homogeneous solution was prepared by dissolving $CuCl_2{\cdot}2H_2O$ (3.35 mmol, 600 mg) and D-(+)-glucose (4.44 mmol, 800 mg) in 40 mL of reverse osmosis water (RO) in a Teflon-lined autoclave. Subsequently, 10 mL of glycerol, 8 mL of oleylamine (OLA), and 0.080 mL of oleic acid (OA) were added. The mixture was stirred at 500 rpm for 10 min at room temperature, then the Teflon-lined autoclave was sealed and placed in a preheated oven at 120–180 °C for 4 h. After cooling to room temperature, the solution was decanted into 50 mL of n-hexane in a separating funnel. After phase separation, the hexane phase containing dispersed CuNWs was collected, and the nanowires were washed by repeated dispersion in fresh hexane and decantation. The resulting nanowires were stored in fresh hexane for further use. In this study, CuNWs were synthesised at the temperatures 120 °C, 140 °C, 160 °C, and 180 °C, and were labelled as CuNW-120, CuNW-140, CuNW-160, and CuNW-180, respectively.

Fabrication of flexible nanofiber surfaces

Nylon-6 (N-6) nanofibers were fabricated via an electrospinning process [27] using a Spinbox® electrospinner (Bioinicia, Spain). A 22 wt % solution was prepared by dissolving N-6 pellets in formic acid. The mixture was sonicated in a bath sonicator for 1 h. For electrospinning the N-6 surface, the resulting solution was loaded into a 10 mL syringe and electrospun for 20–25 min at a flow rate of 1 μL min^{-1}. A metallic surface covered by an aluminium foil was used as the collector for electrospinning the N-6 surfaces. The collector was placed 12–14 cm from the syringe tip and a positive voltage of 17 kV was applied. After electrospinning, the deposited flexible N-6 nanofiber surfaces, measuring thickness ~10–20 μm, were peeled off from the aluminium foil using double-sided tape and used directly for fabricating FCS.

Fabrication of flexible conductive surfaces (FCS)

Vacuum filtration was used to fabricate a copper nanowire (CuNW) based FCS. Electrospun N-6 nanofiber surface was integrated into the filtration setup as the surface onto which CuNWs would be assembled. A suspension of CuNWs (~3 mg mL^{-1}) in hexane (5 mL) was filtered through a circular N-6 substrate. This formed a uniform nanowire film on the N-6 surface that covered a surface area of 9.62 cm^2. The film was treated with 3 mL of a propionic acid: hexane solution (1:29) for 15 s. It was then cleaned twice with 3 mL of ethanol, followed by filtration and drying under vacuum. For stability testing, a polycarbonate (PC) filter membrane was used as the substrate for CuNWs. Hereafter, nanowire/N-6 and nanowire/PC will denote copper nanowires on N-6 and polycarbonate surfaces, respectively.

Fabrication of flexible capacitive curvature sensor

To fabricate the flexible capacitive curvature sensor, two identical pieces of nanowire/N-6 surfaces were considered as electrodes. N-6 nanofiber surface was also used as the dielectric layer with the dimensions 2 cm × 2 cm. The dielectric layer was sandwiched between the two CuNW based nanowire/N-6 surfaces, with their conductive sides facing inward. Then, the sensing region was encapsulated with cellulose tape. The active sensing region was maintained at 1.5 cm × 2 cm.

Characterisations

X-ray diffraction (XRD) analysis was performed using a Panalytical Empyrean X-ray diffractometer equipped with a PIXcel3D solid-state area detector. The scan was conducted over a 2θ range of 30–80° at a scan rate of 2° min^{-1}. X-ray photoelectron spectroscopy (XPS) was carried out using a Thermo Scientific Nexsa instrument equipped with a monochromatized Al Ka X-ray source and dual-beam charge compensation system. The survey and high-resolution spectra were scanned using 200 eV and 50 eV pass energies, respectively. All the spectra acquired were deconvoluted using the CasaXPS curve fitting software using Shirley background and were corrected for charge-shift with reference to the adventitious carbon positioned at 284.8 eV. The morphology of the synthesised nanowires and the nanowire/N-6 FCS was examined using a field-emission scanning electron microscope (FE-SEM, Apreo S, Thermo Fisher Scientific) operated at acceleration voltages of 2 kV and 5 kV. SEM imaging was done mainly using secondary electron detectors. SEM was used for the imaging of nanowire/N-6 FCS. Energy-dispersive X-ray spectroscopy (EDS) was performed to analyse the elemental composition of the nanowire/N-6 FCS using the same SEM. The structural characterisation of the CuNWs was performed using a JEM-1400 Plus transmission electron microscope (TEM) operated at 80 kV. Additionally, high resolution TEM imaging and morphological analysis was performed in a JEOL JEM-F200 TEM operated at 200 kV voltage. A TA.XT.plus100C texture analyser was used for the capacitive curvature sensing and cyclic durability tests of the nanowire/N-6 sensors. The relative change in resistance and capacitance was measured using an LCR meter (GW-INSTEK LCR-6300). A testing signal of 1 V at 1 kHz was applied for all LCR meter measurements. The sheet resistance of the flexible conductive surfaces was measured using an Ossila four-point probe system with a probe spacing of 1.27 mm.

Results and discussion

Synthesis and characterisations of nanowires

In this work, we synthesise ultra-long copper nanowires (CuNWs) to enhance the durability of flexible sensors. CuNWs were prepared by a simple solution-phase polyol route [24] in a sealed autoclave, using a water-glycerol solvent system in which the copper (II) salt was dissolved. Glucose served as the reducing agent to convert Cu(II) to metallic Cu(0), while oleylamine and oleic acid functioned as capping/directing ligands to promote anisotropic and one-dimensional growth into

ultra-long wires. The reaction temperature was systematically varied from 120 to 180 °C to tune nanowire quality including aspect ratio, crystallinity, and surface smoothness to improve stability relevant to durable flexible electronics. A schematic comparison of the resulting morphologies at each synthesis temperature is shown in the schematic of Fig. 1.

Fig. 1 (a-d) shows SEM images of nanowires synthesised from 120 to 180 °C. At lower temperatures, the nanowires appeared to have smaller diameters, however, they become larger and smoother at higher temperatures. The average diameters were also determined from measurements of ~100 nanowires from SEM images. The diameters are 43 ± 6 nm, 61 ± 18 nm, 66 ± 27 nm, and 74 ± 31 nm for CuNW-120, CuNW-140, CuNW-160 and CuNW-180 respectively. Corresponding Gaussian-fitted histograms are shown in the insets of **Fig. S1 (a-d)**. Following this, the average lengths were also measured from SEM images, which are 24 ± 13 μm, 83 ± 31 μm, 128 ± 32 μm and 64 ± 18 μm for CuNW-120, CuNW-140, CuNW-160 and CuNW-180 respectively. The results are shown in SEM images in **Fig. S2 (a-d)** and plotted in **Fig. S3** together with diameter distribution. The length-to-diameter (L/D) aspect ratios of the nanowires were calculated as 558, 1356, 1939, and 865, respectively. The L/D ratio of the nanowires was observed to have an increasing trend up to a maximum aspect ratio of 1939 at 160 °C, however at 180 °C, the L/D ratio was significantly reduced. Further, TEM images were acquired as shown in Fig. 1 (e-h), reflecting increasing in diameters at higher temperatures. Insets (top) in Fig. 1 (e–h) present the corresponding high-resolution micrographs with visible lattice spacings. For CuNW-120, we could observe two crystal planes from the core and surface of the nanowires, the measured lattice spacings are d_{111} ~ 0.21 nm and d_{111} ~ 0.24 nm, respectively. These lattice spacings were identified to be (111) crystalline planes for Cu and the oxides. However, such oxidised phases were gradually reduced at higher temperatures. Further, selected area electron diffraction (SAED) patterns were obtained as shown in bottom insets of Fig. 1 (e-h), indicating the nanowires are of crystalline nature [28]. In an earlier study, Yu Shi et al., reported improved crystallinity at higher reaction temperatures beyond 160 °C due to faster rate of thermodynamic diffusion [29]. To investigate the crystal properties, X-ray diffraction (XRD) patterns were obtained, as shown in Fig. 2a. All the nanowires showed three dominant reflections at 2θ ~ 43.3°, 50.5°, and 73.5° corresponding to the (111), (200), and (220) planes of copper [30]. According to the JCPDS 04–0836, the nanowires are composed with a face centred cubic (FCC) crystalline lattice. In addition, the crystallite size was calculated using the Scherrer equation, as shown in Eq. (1) [31]. The average crystallite sizes for the Cu (111) facet were determined. Accordingly, crystallite sizes were measured to be 15 ± 0.8, 17 ± 1.5, 21 ± 2.3, and 17 ± 0.5 nm, respectively for CuNW-120, CuNW-140, CuNW-160, and CuNW-180. These results indicate that the crystallite size (D_{111}) was initially small and reached a maximum in the case of CuNW-160. Smaller crystallite size increases the density of grain boundaries, which serve as rapid diffusion pathways for oxygen. On the contrary, as crystallite size grows, boundary density decreases, rendering the material less susceptible to aerobic oxidation [32].

$$\textit{Crystallite size}\ (D_{111}) = \left(\frac{\lambda \times K}{\beta \times \cos\theta}\right) \quad (1)$$

Where, β = full width at half maximum (FWHM) (in radians); Scherrer's constant $K = 0.94$; λ = X-ray source wavelength = 0.15406 nm; θ = angle of diffraction.

Furthermore, CuNW-120 shows a weak diffraction peak at 2θ ~ 36.3° which is attributed to the presence of Cu_2O (111) (JCPDS 05–0667) in minor quantities [33]. The presence of oxide phase is also evidenced from the high-resolution TEM images (top insets in Fig. 1 (e-h)). However, such oxide layer was reduced at the temperatures beyond 140 °C.

To analyse surface oxidation states, the nanowires were examined by X-ray photoelectron spectroscopy (XPS). The high-resolution Cu 2p spectra (Fig. 2c) show an intense spin-orbit doublet in the range ~930–960 eV. They are separated by ~19.8 eV with an area ratio close to 2:1 characteristic of copper. Deconvolution of the CuNW-120 spectra

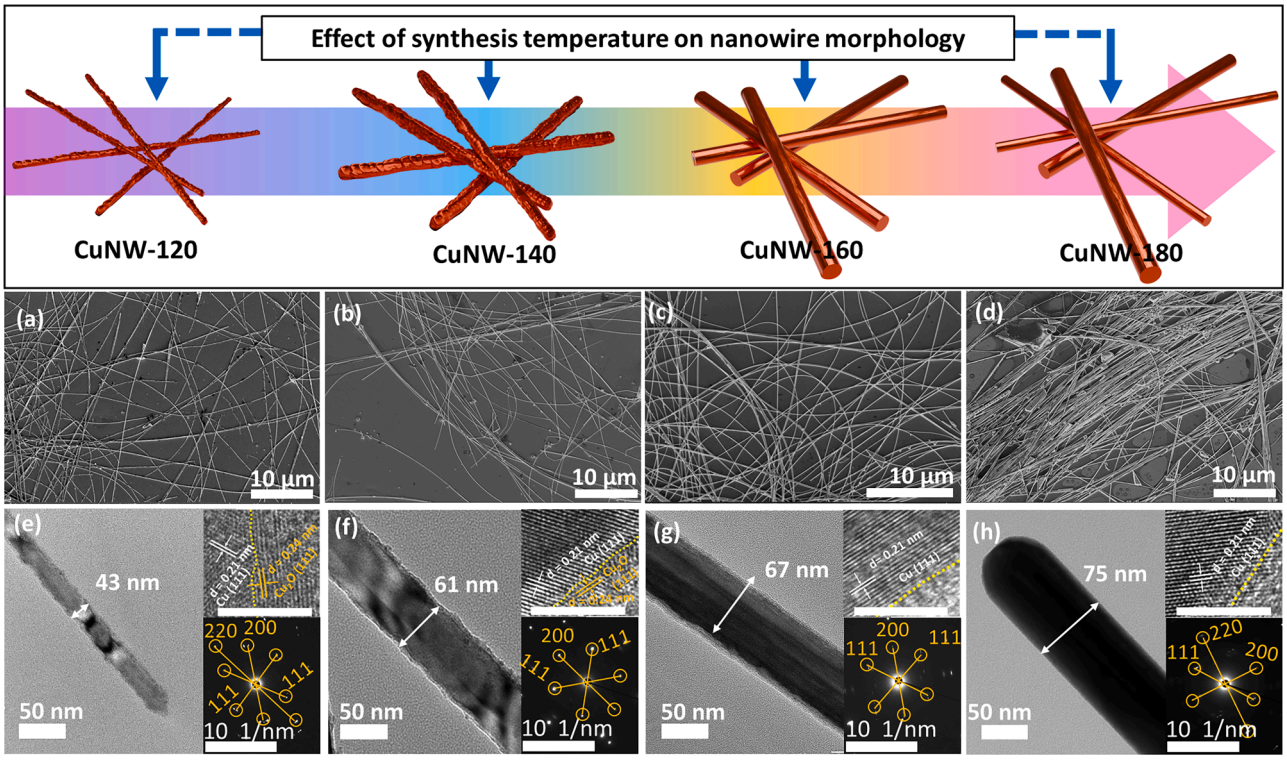

Fig. 1. Temperature dependent morphology of copper nanowires. From left to right: CuNW-120, CuNW-140, CuNW-160, and CuNW-180: (a–d) SEM images, (e–f) TEM images with HR-TEM micrographs (top-right insets: scale bar: 5 nm) and SAED patterns (bottom-right insets).

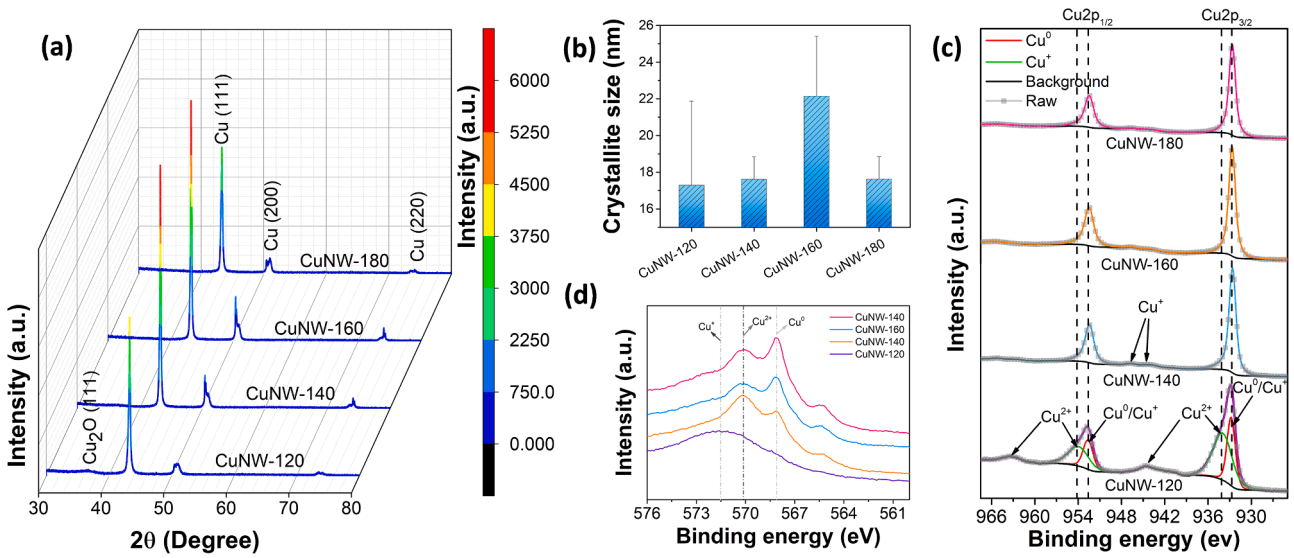

Fig. 2. Characterisation of CuNW-120, CuNW-140, CuNW-160, and CuNW-180: (a) XRD patterns, (b) comparison of crystallite sizes, (c) Cu 2p narrow scans and (d) Cu LMM Auger spectra.

reveals additional components at ~934.2 eV ($2p_{3/2}$) and ~954.2 eV ($2p_{1/2}$). These shifted by ~1.4 eV relative to the Cu^0 peaks which is attributable to the presence of native surface oxides which is also validated from a shake-up satellite peak at ~939–948 eV [34]. The Cu LMM Auger spectra (Fig. 2d) further corroborate the coexistence of Cu^0, Cu^+ and Cu^{2+} oxidation states in all the samples. However, the Cu° fraction increases at elevated synthesis temperatures, ascribing to more effective reduction of the copper precursor at elevated temperatures. The survey spectra (**Fig. S4**) indicates that the nanowires comprise only of copper (Cu), oxygen (O), and carbon (C). The thin layer of C and O is common for Cu nanostructures prepared via wet-chemical process, which is formed from adsorbed organic residues and slight surface oxidation [16]. Traces of chlorine (Cl) were also detected, likely originating from some of the $CuCl_2$ precursor being weakly adsorbed onto the nanowire surface.

Overall, the temperature dependence of morphology and chemical composition of nanowires were also aligning with earlier studies. Hemmati et al. showed that higher temperatures accelerate Ag^0 nucleation via rapid ethylene glycol to glycolaldehyde conversion [35]. This reflects that lower reaction temperatures (120 – 140 °C) could possibly lead to insufficient reduction of Cu^{2+} from the precursor to metallic Cu^0 nanowires, as evidenced from the XPS and high-resolution TEM images. As a result, nanowires appeared narrower, shorter and had high surface roughness. At higher temperatures, growth proceeds along both the length and side facets, producing longer and wider nanowires. This was also evidenced from the increasing crystallite sizes derived from XRD, leading to the formation of smoother ultra-long nanowires till 160 °C [36]. At 180 °C, the nanowires were smooth, but irregular dimensions were observed. Basarir et al. confirms the decomposition of glucose into carbonised form at temperatures beyond 160 °C, which facilitates shorter nanowire formation [37]. If so, the nanowires would exhibit more oxidised surfaces at 180 °C because of insufficient reduction. However, we observed an increasing Cu^0 than its higher oxidation states Cu^+ in CuLMM spectra as the temperature increased which does not align with the glucose carbonisation. Moreover, no carbonised coating appeared in the high-resolution TEM micrographs at 160 and 180 °C. Instead, the partial decomposition of the oleylamine/oleic acid (OLA/OA) capping agent pair could be a more closely applicable explanation for our results [38]. OLA/OA pair binds to the metal facets based on the surface-energy order, which is (111) < (100) < (110) [30]. Therefore, side facets i.e. (100), which are responsible for controlling diameter, are preferentially passivated for further growth. This produces narrower diameters, elongated nanowires, and a larger crystal size at elevated temperatures. Altogether, at 180 °C, the partial decomposition of OLA/OA likely disrupts this adsorption-desorption equilibrium, relaxing facet selectivity and leading to uncontrolled growth and broader size distributions and reduction of crystallite size.

Performance and durability of nanowire assessment

To be able to use in flexible electronics, nanowires should be uniformly assembled on a flexible surface and maintain good electrical conductivity. As the nanowires tend to aggregate in solutions due to their high surface energy, it is crucial to choose the right approach carefully to assemble them [39]. Vacuum filtration is a simple approach which provides percolated nanowire networks on a surface. Further, the percolated nanowire networks can be easily transferred onto any substrates of interest. Accordingly, the nanowires were assembled on a polycarbonate (PC)-based surface via vacuum filtration process. We prepared four nanowire network/PC -based conductive surfaces (CS). PC substrates were chosen as a model platform to evaluate electrical, thermal, and humidity stability of the CuNW networks, while N-6 nanofiber mats were used for flexible device integration due to their mechanical compliance and role as both substrate and dielectric in capacitive sensors [55].

In the beginning, we measured the electrical conductivities of the nanowire/PC surfaces. However, all of them showed poor electrical conductivity typically in the range of 0.5–10 MΩ. This often happens when metal nanowires are prepared using wet chemical process due to the formation of an oxide or carbon layer [16]. This creates an insulating encapsulation on the nanowires that protects from ohmic contact between the nanowires leading to high junction resistance [40]. To remove such encapsulations, nanowire surfaces are often post treated using high temperature annealing, which is not compatible with most flexible surfaces. The nanowire/PC surfaces were treated using diluted propionic acid (PA) followed by vacuum filtration [14]. This approach resulted in reaching low sheet resistances of about 9–30 Ω sq^{-1}, which was measured using a four-probe system from five different spots of each nanowire/PC surface. A typical measurement setup is shown in Fig. 3a.

For durable flexible electronics, conducting nanowires must maintain low electrical resistance and mechanical integrity across various environments. To investigate oxidative stability, the nanowire/PC surfaces were stored under ambient conditions (25 °C, ~35 % RH). Faster oxidation resulted in an increase in sheet resistance. Here, SR_0 = average

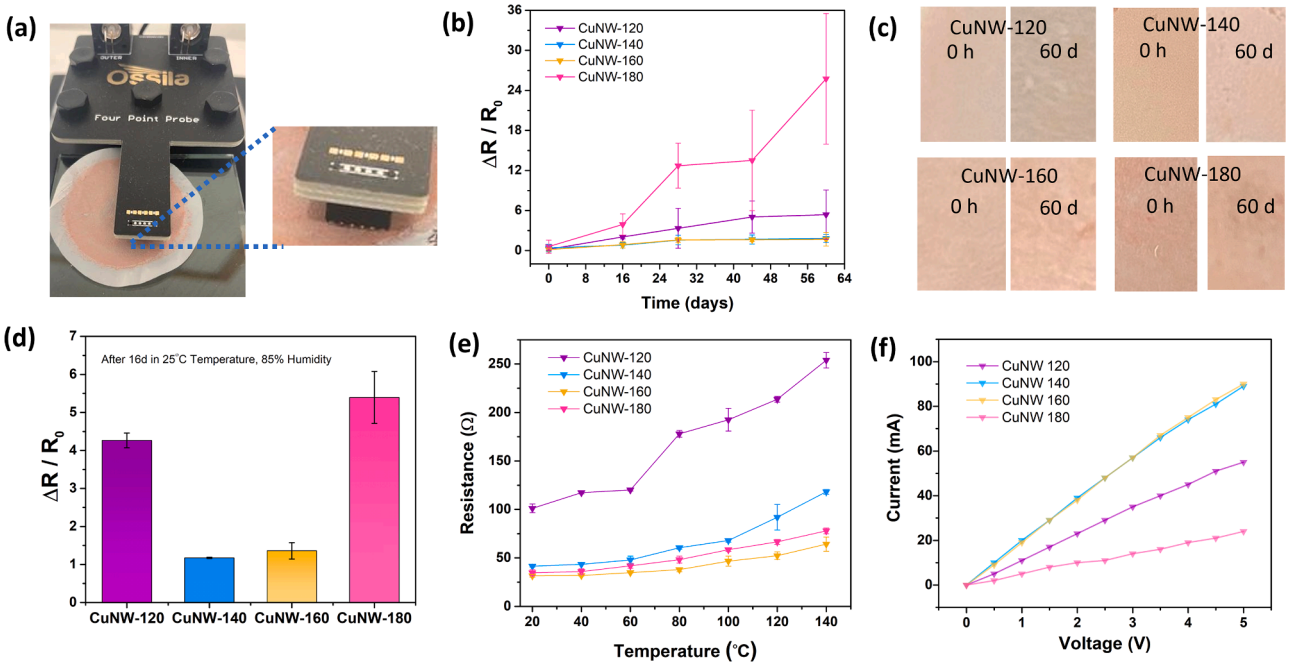

Fig. 3. (a) Setup for sheet-resistance measurement with an Ossila four-point probe, (b) relative sheet resistance change ($\Delta R/R_0$) over time for CuNW/PC surface at ambient conditions (25 °C, ~35 % RH), (c) visual appearance of nanowire/PC surface at 0 h and after 60 days in ambient conditions, (d) relative sheet resistance change after 16 days in a weather chamber set at 25 °C and 85 % RH, (e) temperature dependence of resistance, and (f) I-V characteristics of nanowire/PC surfaces.

sheet resistance for fresh sample (i.e. 0^{th} day) and SR_i = average sheet resistances on i^{th} day. For averaging the sheet resistance, five measurements were taken at five different spatial positions on each CuNW/PC sample. The relative sheet resistance was calculated based on the following equation:

$$\frac{\Delta R}{R_0} = \frac{SR_i - SR_0}{SR_0} \quad (2)$$

In Fig. 3b CS fabricated with CuNW-140 and CuNW-160 showed the best retention of conductivity, with $\Delta R/R_0$ values of only ~1.7 and ~1.8, respectively. In contrast, the CuNW-120 and CuNW-180 based CS, showed markedly larger increases in $\Delta R/R_0$ which were approximately 5.4 and 26. This indicates that CuNW-160 showed superior oxidative stability. Further, to examine the intermediate-stage oxidation of the nanowire surfaces, XPS data were collected after 28 days (**Fig. S5**), revealing features attributable to Cu^0 and Cu^{2+} species in all nanowires. Notably, the Cu^{2+} contribution was higher for CuNW-120 and CuNW-180. After 60 days, photographs of the nanowire surfaces were acquired, showing noticeable colour changes in the CuNW-120/PC and CuNW-180/PC samples compared to the fresh samples (Fig. 3c). CuNW-120/PC developed a grey shade and CuNW-180/PC darkened, both characteristic of Cu oxidation [25]. In contrast, the CuNW-140/PC and CuNW-160/PC surfaces showed no visible change was observed which is validating stable resistance.

Humidity accelerates CuNW oxidation by providing water vapor that dissociates at grain boundaries and rough surfaces, forming hydroxyl species (e.g., Cu-OH) that enhance oxygen dissociation and ingress via the reaction $H_2O + O_{ads} \rightarrow 2OH_{ads}$ [41]. This catalytic effect increases effective oxygen diffusivity by several times as compared to dry ambient air. Consequently, a shorter period is required at higher relative humidity than ambient exposure. Therefore, to evaluate their stability under such extreme conditions, the nanowire/PC surfaces were further stored in a weathering chamber at 25 °C and 85 % relative humidity (RH). The relative change in sheet resistance ($\Delta R/R_0$) was monitored over 16 days (Fig. 3d). After 16 days, $\Delta R/R_0$ values were approximately 4.3, 1.2, 1.4, and 5.4 for CuNW-120, CuNW-140, CuNW-160, and CuNW-180, respectively. CuNW-120/PC and CuNW-180/PC exhibited remarkable increase in $\Delta R/R_0$ values which indicates poor moisture stability. In contrast, a smaller increase was observed for CuNW-140/PC and CuNW-160/PC, retaining conductivity with minimal degradation under high humidity. Notably, CuNW-140/PC and CuNW-160/PC maintain high stability, approaching that of encapsulated systems, demonstrating performance competitive with existing literatures [42]. For example, a CuNW electrode encapsulated in a polyurethane acrylate layer fabricated by Kim et al., showed relative change in sheet resistance ($\Delta R/R_0$) of ~3 after 4 h in high temperature and high humidity (80 °C, 80 % RH) [42].

After we subjected the nanowire/PC surfaces that had been 16 days in the weather chamber to 10,000 bending cycles and then stored them for ~1 month. SEM imaging showed that nanowire morphology remained largely preserved over this period (**Fig. S6 a-d**). However, after ~3 months of storage in ambient conditions, the CuNW-120/PC surface displayed clear morphological changes (**Fig. S6 e-h**). On the other hand, CuNW-140/PC, CuNW-160/PC, and CuNW-180/PC appeared unchanged, indicating that CuNW-120 is more susceptible to oxidative degradation.

The thermal stability of nanowire/PC surfaces was assessed from 20 °C to 140 °C which is shown in Fig. 3e. CuNW-120/PC showed low sheet resistance at lower temperatures, but resistance began increasing above ~60 °C. In contrast, CuNW-160/PC maintained low resistance up to 140 °C, indicating superior thermal stability relative to the other samples. Thermally induced failure pathways given their Rayleigh (capillary) instability that drives nanowire spheroidization and thermally accelerated oxidation (Fig. 3e) [43]. These processes often co-occur, intensifying degradation. In our CuNW/PC surface, the observed changes may also be influenced by thermal softening of the PC substrate, which could promote nanowire rearrangement and oxidation [43].

To further elucidate the structural origin of the enhanced stability, we evaluated how crystallite size and surface roughness influence oxidation kinetics. The average crystallite size (D_{111}) increased from 15 nm for CuNW-120 to 21 nm for CuNW-160, corresponding to an ~1.4-fold reduction in grain-boundary area per unit volume. Since grain boundaries act as high-diffusivity pathways for oxygen, this reduction is expected to lower the effective oxygen diffusivity. Based on the reported

proportionality between the oxidation rate constant (k_o×) and grain-boundary density in nanocrystalline Cu, the effective oxygen diffusivity is estimated to decrease by several times [44,45]. Consistent with this trend, CuNW-160 exhibits a two-fold or greater suppression in resistivity increase at the corresponding aging times. Moreover, oxygen diffusivity is more pronounced in narrower nanowires synthesised at lower temperatures, where rapid surface and bulk oxidation create rougher surface morphologies and thus an exponential increase in $\Delta R/R_0$ at longer exposure periods [46]. In contrast, the smoother surfaces of CuNW-160 effectively suppress oxygen adsorption and oxidation initiation sites, eliminating such exponential behaviour. Together, reduced grain-boundary diffusion and lower surface reactivity explain the superior environmental stabilities of CuNW-160 compared to other samples in both ambient and higher humidity. Prior studies further confirm that crystallite size governs both electrical noise (from dynamic grain boundaries) and mechanical flexibility, supporting our analysis [47,48].

The electrical robustness of the nanowire/PC films was evaluated by current-voltage (I-V) measurements (Fig. 3f). All samples display linear I-V characteristics confirming ohmic behaviour. The electrical conductivity trend is CuNW-160 ~ CuNW-140 >> CuNW-120 >> CuNW-180. CuNW-140 and CuNW-160 carry the highest electrical currents over 0–5 V, which is consistent with highly percolated networks forming good junction contacts owing to the longer nanowires. The high electrical conductivity is still linearly maintained even at high voltage which indicates that the nanowires are stable under higher voltages without loss in electrical performance. In contrast, CuNW-180 shows the lowest slope, reflecting poorly fused junctions and shorter or less uniform nanowires that reduce parallel conduction paths. CuNW-120 is intermediate, suggesting higher intrinsic and/or junction resistance. Additionally, its lower conductivity may appear from an insulating oxide layer at the nanowire surface that elevates junction resistance.

To evaluate suitability for flexible electronics, we measured resistance as a function of curvature using a texture analyser and LCR meter (**Fig. S7 a-b**). All nanowire/PC surfaces remained operational across the range of 124–489 m^{-1}. CuNW-160/PC showed the most robust performance with only a 0.6 Ω change in resistance even at 489 m^{-1} resulting from a mechanically resilient connection. CuNW-180/PC was also largely curvature-insensitive but exhibited a higher baseline than CuNW-160/PC. In contrast, CuNW-120/PC had a much higher resistance that increased sharply beyond ~369 m^{-1} and CuNW-140/PC remained stable until ~445 m^{-1} before increasing, consistent with strain-induced junction failure. The deviation from the usual "thinner-is-more-flexible" expectation likely arises due to differences in junction quality, surface smoothness, and emerging oxidation (particularly in CuNW-120), which elevate intrinsic and contact resistances under bending [49].

To benchmark stability, we compared our CuNW-160/PC surfaces with representative reports from the literature (**Table S1**, supporting information). In studies using uncoated CuNWs for flexible conductive surfaces, Chu et al., Rathmell et al., and Yin et al. reported conductivity retention for 38, 28, and 7 days, respectively, under ambient conditions, whereas our CuNW-160/PC maintained $\Delta R/R_0 \approx 1.8$ for over 60 days [19,30,50]. Even compared to encapsulated systems, our results remain highly competitive. For example, CuNWs sandwiched in PES/PET retained $\Delta R/R_0 \approx 1$ over 45 days, TiO_2-coated CuNWs exhibited $\Delta R/R_0 \approx 2$ over 30 days, and CuNW conductive tapes showed stability of only 7 days [25,26]. Notably, our CuNW-160 achieves comparable long-term stability without the use of protective coatings or encapsulation layers. This highlights the advantage of achieving oxidation resistance through intrinsic microstructural optimization rather than additional processing steps, preserving both simplicity and cost-effectiveness.

In summary, the stability of electrical conductivity in metal nanowires is altered by structural and surface parameters including surface oxidation state, length and diameter, crystallite size, and surface roughness [51,52]. Smaller diameters restrict the number of conducting electrons and amplify surface-electron scattering, raising resistance. This effect is most pronounced in thin, rough nanowires such as in CuNW-120/PC [52]. On the contrary, thicker nanowires with smoother surfaces mitigate surface scattering which is accountable for the superior stability of CuNW-160/PC. CuNW-160 also exhibits the largest crystallite size, which reduces grain-boundary scattering and limits reactive sites for oxidative degradation [44]. Although CuNW-180/PC shows a relatively smooth and less oxidised surface, its stability is compromised by broad dispersity in length and diameter which weakens network percolation and increases junction resistance.

Capacitive curvature sensor application

Given their promising environmental stability (particularly for CuNW-140/160), the nanowire networks exhibited comparable stability. To compare their mechanical robustness under bending, we fabricated flexible capacitive curvature sensors. Highly stable flexible capacitive sensors are widely investigated for portable touch and motion detection (e.g., finger, arm, or knee bending) [53]. Accordingly, we constructed curvature sensors using each nanowire network to evaluate their practical applicability. A typical approach for fabrication of nanofiber-based flexible capacitive curvature sensor is shown in Scheme 1.

The copper nanowires and N-6 nanofibers are clearly distinguishable in SEM image. To analyse the elemental composition of the FCS, energy dispersive X-ray spectroscopy (EDS) was used as shown in Fig. 4 (a-d). As expected, carbon, nitrogen and oxygen were present from the N-6 nanofibers and copper was present in nanowires, indicating effective integration of CuNWs onto the N-6 nanofiber surface.

In the flexible capacitive curvature sensor, electrospun N-6 nanofiber surface was used as the dielectric layer sandwiched between two conducting FCS, to provide insulation and prevent short-circuiting. During testing, the device was bent, and the relative capacitance change ($\Delta C/C_0$) was recorded with a combined interface of a texture analyser, LCR meter and MATLAB. The sensor responds with a change in capacitance when there is a change in curvature of the sensor. As the sensor bends, the separating distance between the two FCS decreases in the active region and the capacitance increases. This happens due to the simultaneous effect of tensile strain on outer surface and compressive strain on inner surface while bending. This curvature induced variation in electrode separation produces a corresponding change in overall capacitance value of the sensor making it a curvature sensor. The sensor responds similarly to parallel plate capacitor equation as shown in Eq. (3) [54].

$$C = \frac{\varepsilon \times A}{d} \tag{3}$$

Where, C = capacitance in Farads, ε = permittivity of dielectric medium, A = Area of the active region in square meters and d = distance between the electrode surfaces in metres.

Accordingly, all the sensors were subjected to 10,000 bending cycles on the day of fabrication (0^{th} day), as shown in Fig. 5. The sensors initially showed strong $\Delta C/C_0$ signals during compression and relaxation cycle. With continued cycling, CuNW-160/N-6 and CuNW-140/N-6 displayed the most stable response which remained constant with negligible signal noise, indicating a durable percolation nanowire network. In contrast, CuNW-180/N-6 exhibited a gradual decay of response over the first several thousand cycles with transient spikes possibly due to evolving interfacial slip or microcrack formation. The expanded cycles (990–1000 and 8820–8830) are shown in Fig. 5 indicating irreversible signals of CuNW-180/N-6 based sensor. CuNW-120/N-6 showed higher sensitivity but unpredictable noisy trend throughout overall bending cycles indicating irregular junction failure and unreliable sensing even after having larger $\Delta C/C_0$ value. Overall, the bending-durability ranking is CuNW-160 ≥ CuNW-140 >> CuNW-180 > CuNW-120, with CuNW-160/140 providing the best combination of stability

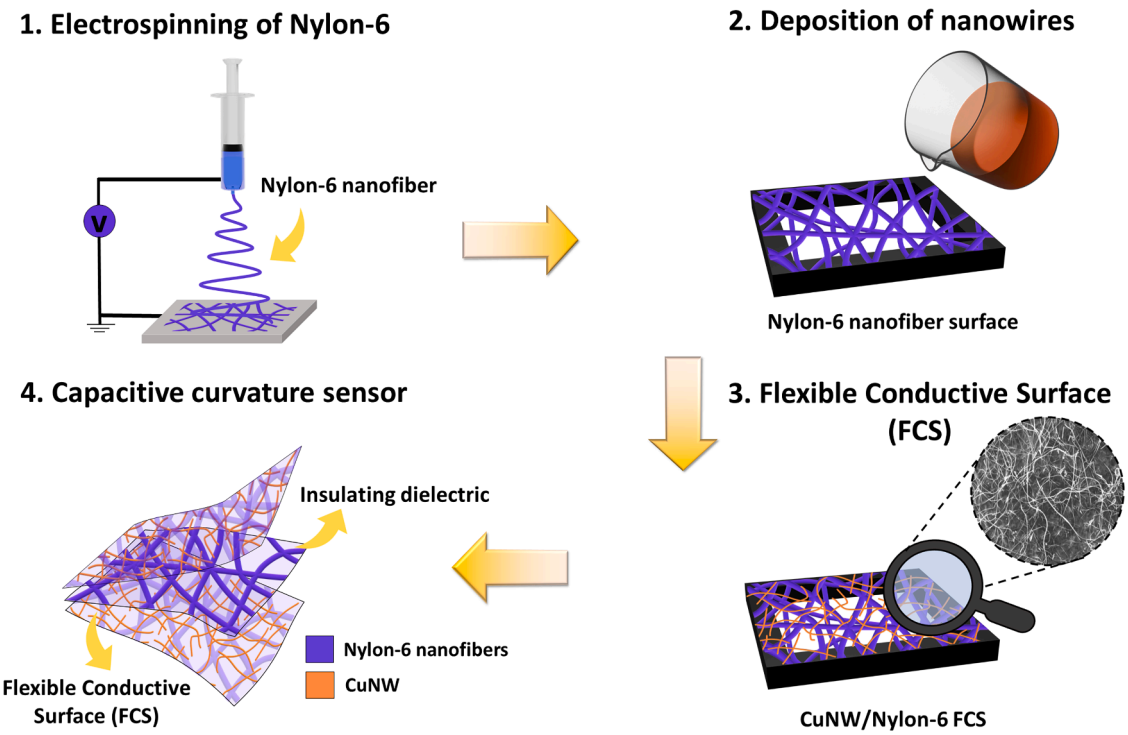

Scheme 1. Schematic of curvature-sensor fabrication: 1. electrospinning nylon-6, 2. vacuum-filtering nanowires onto the nylon-6 surface, 3. representation of nanowires/nylon-6 based flexible conducting surface, and 4. integrating into a capacitive curvature sensor.

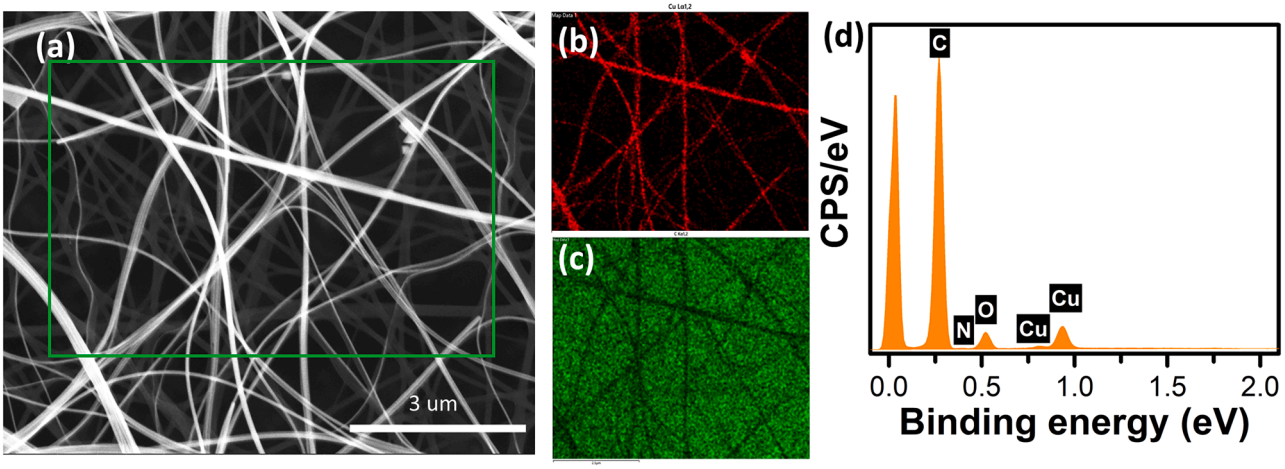

Fig. 4. SEM analysis of CuNW-160/N-6 FCS and electrical characterisation of curvature sensor: (a) micrograph with the EDS elemental mapping overlay area shown in the green box (b) Cu from nanowires and (c) N from Nylon-6, Capacitive curvature sensors (d) EDS spectrum of elemental mapping overlay area shown in Fig. 4a.

and reliability. A quantitative comparison of sensitivity, curvature range, and cycling durability with previously reported flexible curvature and strain sensors is provided in **Table S2**.

Furthermore, we acquired curvature response over aging at ambient conditions. **Fig. S8** shows the normalised capacitance change ($\Delta C/C_0$) versus curvature (κ) ranging from 0–450 m^{-1}. CuNW-140 and CuNW-160 show an almost linear $\Delta C/C_0$ - κ relationship over the curvature at 0^{th} day, which are desirable bending statistics. The linearity is still maintained with only a modest drop in sensitivity after storing them for 75 days. This result indicates an excellent stability. However, CuNW-180 shows a moderate, nonlinear response at 0^{th} day but undergoes a marked reduction in sensitivity within 14 days (**Fig. S8**) which is also consistent with the transient spikes observed in the cyclic tests. In fact, CuNW-120 outperformed the other sensors with the highest initial sensitivity, but a meaningfully nonlinear response was observed that reflects a highly compressible electrode network. Although, the response remained higher than that of the other nanowires, it decreased relative to its initial value after 14 days. When combined with its noisy behaviour under cycling, this profile indicates an improved sensitivity than CuNW obtained at higher temperatures from 140 to 180 °C but poor reliability for precise measurement. For practical applicability and reliable curvature sensing, CuNW-160 and CuNW-140 offer the best balance, stable and near-linear sensitivity that perseveres after extended aging, while CuNW-180 is limited by aging-related loss of sensitivity and CuNW-120, despite large signals, is inhibited by nonlinearity and unreliable dynamics.

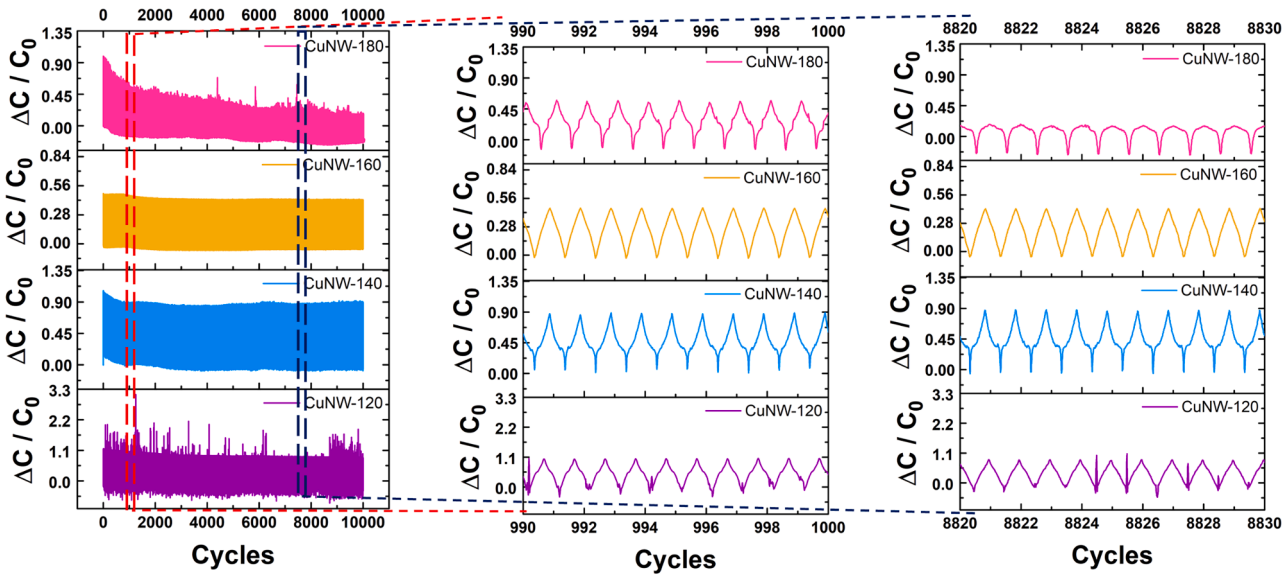

Fig. 5. $\Delta C/C_0$ vs. bending cycles for durability tests under 10,000 bending cycles for CuNW-120/140/160/180, with insets magnified to cycles 990–1000 and 8820–8830.

Conclusions

In conclusion, we synthesised copper nanowires at 120, 140, 160, and 180 °C, characterised their properties, and evaluated structure-property-stability relationships with the goal of fabricating highly durable flexible sensors. The nanowires prepared at lower temperatures were narrower and shorter, exhibited poorer crystallinity, and showed relatively rough surfaces with thicker Cu_2O layers. At higher temperatures, the nanowires became longer and wider, more crystalline, and smoother, with fewer surface defects and thinner oxide layers. Beyond ~160 °C, irregular morphologies appeared, likely due to the thermal decomposition of oleylamine and oleic acid.

Durability was examined by fabrication of flexible conducting surfaces using electrospun nylon-6 nanofiber and polycarbonate-based surfaces. The conducting surfaces underwent several assessments including electrical, chemical and mechanical stabilities. The nanowires prepared at intermediate temperatures (140 °C and 160 °C) outperformed the others under diverse environmental conditions. They maintained consistent sheet resistance for over 60 days at ambient conditions (25 °C, ~35 % RH), showing stability comparable to, and in some cases exceeding, that of reported nanowires, including encapsulated nanowires. These nanowires also survived under extreme conditions, including high humidity (85 % RH), heat exposure up to 140 °C, and voltage bias up to 5 V. Furthermore, the nanowire-based surfaces, other than CuNW-120/PC, exhibited stable resistance at a near maximum curvature of 445 m^{-1}. All CuNW-based sensors, other than that based on CuNW-180, retained stable capacitive sensitivity over 10,000 bending cycles at a curvature of 450 m^{-1}. Overall, CuNWs synthesised at 140 °C and especially 160 °C provide the best combination of electrical, environmental, and mechanical stability, whereas 120 °C and 180 °C yield nanowires with significantly inferior performance.

The nanowire stability can be effectively tuned via careful control of the reaction temperature. Although, copper nanowires are prone to rapid oxidation which has limited their adoption in flexible electronics, optimising the synthesis temperature substantially minimises this barrier. This study identifies synthesis temperature as a simple and effective parameter for improving the stability and durability of CuNWs. Temperature regulates reduction kinetics, nucleation, and surface diffusion, thereby controlling nanowire morphology and defect density. While the approach is broadly applicable, the optimal temperature depends on the reducing agent and capping ligand used. Consequently, temperature tuning is a general strategy that must be adapted to the specific chemical environment of each synthesis system. Therefore, this work addresses a key bottleneck strategy for the creating highly durable nanowires for flexible electronic applications.

CRediT authorship contribution statement

Linda Broere: Writing – original draft, Visualization, Software, Methodology, Investigation, Formal analysis, Data curation. **Rituporn Gogoi:** Writing – review & editing, Writing – original draft, Visualization, Validation, Supervision, Methodology, Investigation, Formal analysis, Conceptualization. **Amit Barua:** Software, Methodology, Investigation, Formal analysis, Data curation. **Nidhin George Mathews:** Visualization, Validation, Formal analysis. **Sari Granroth:** Visualization, Validation, Methodology, Formal analysis. **Kristofer Kolpakov:** Software, Formal analysis, Data curation. **Gaurav Mohanty:** Writing – review & editing, Resources, Project administration, Investigation, Funding acquisition, Formal analysis. **Emilia Peltola:** Validation, Resources. **Vipul Sharma:** Writing – review & editing, Validation, Supervision, Resources, Project administration, Funding acquisition, Conceptualization.

Declaration of competing interest

The authors declare that they have no known competing financial interests or personal relationships that could have appeared to influence the work reported in this paper.

Acknowledgements

This work is supported by financial assistance from the project DURATRANS (364364, 2024–2027) under the framework of M-ERA.net. The authors are grateful to the Materials Research Infrastructure (MARI) at the University of Turku and Tampere Microscopy Center at Tampere University for providing infrastructural facilities. Rituporn Gogoi acknowledges SUSMAT for the research funding. We thank Ilari Angervo for assistance with X-ray diffraction measurements. We also thank Ermei Mäkilä for assistance in scanning electron microscopy, Markus Peurla for support in transmission electron microscopy and Shaharyar Siddique for support in sensor fabrication. Gaurav Mohanty and Nidhin George Mathews also acknowledge partial support from the project HERBIE

(341050, 2021-2025) funded by Research Council of Finland. During the preparation of this work, the author(s) used ChatGPT 5.2 to improve readability and language. After using this tool/service, the author(s) reviewed and edited the content as needed and take(s) full responsibility for the content of the publication.

Supplementary materials

Supplementary material associated with this article can be found, in the online version, at doi:10.1016/j.ceja.2026.101111.

Data availability

Data will be made available on request.

References

[1] Y. Yu, J. Li, S.A. Solomon, J. Min, J. Tu, W. Guo, C. Xu, Y. Song, W. Gao, All-printed soft human-machine interface for robotic physicochemical sensing, Sci. Robot. 7 (2022) eabn0495.
[2] J.M. Perkel, THE INTERNET OF THINGS COMES TO THE LAB - the system of connecting machines and sensors is finally making its way into the laboratory, giving researchers peace of mind and restoring their work-life balance, Nature 542 (2017).
[3] K.A. Mirica, Unlocking the potential of wearable sensors in healthcare and beyond, ACS Sens. 9 (2024) 533–534, https://doi.org/10.1021/acssensors.4c00325.
[4] G. Verma, S. Sarma, E. Koch, A. Dietzel, Flexible touch and gesture recognition system for curved surfaces with machine learning for assistive applications, Sens. Actuators Rep. 9 (2025), https://doi.org/10.1016/j.snr.2025.100284.
[5] P. Wang, M. Hu, H. Wang, Z. Chen, Y. Feng, J. Wang, W. Ling, Y. Huang, The evolution of flexible electronics: from nature, beyond nature, and to nature, Adv. Sci. 7 (2020), https://doi.org/10.1002/advs.202001116.
[6] M. Saquib Sarwar, Y. Dobashi, C. Preston, J.K.M. Wyss, S. Mirabbasi, J. David, W. Madden, Bend, stretch, and touch: locating a finger on an actively deformed transparent sensor array, Sci. Adv. 3 (2017). https://www.science.org.
[7] Y. Ding, S. Xiong, L. Sun, Y. Wang, Y. Zhou, Y. Li, J. Peng, K. Fukuda, T. Someya, R. Liu, X. Zhang, Metal nanowire-based transparent electrode for flexible and stretchable optoelectronic devices, Chem. Soc. Rev. 53 (2024) 7784–7827, https://doi.org/10.1039/d4cs00080c.
[8] H. Ha, C. Amicucci, P. Matteini, B. Hwang, Mini review of synthesis strategies of silver nanowires and their applications, Colloids Interface Sci. Commun. 50 (2022), https://doi.org/10.1016/j.colcom.2022.100663.
[9] J. Wang, Z. Zhang, S. Wang, R. Zhang, Y. Guo, G. Cheng, Y. Gu, K. Liu, K. Chen, Superstable copper nanowire network electrodes by single-crystal graphene covering and their applications in flexible nanogenerator and light-emitting diode, Nano Energy 71 (2020), https://doi.org/10.1016/j.nanoen.2020.104638.
[10] F. Qian, P.C. Lan, T. Olson, C. Zhu, E.B. Duoss, C.M. Spadaccini, T.Y.J. Han, Multiphase separation of copper nanowires, Chem. Commun. 52 (2016) 11627–11630, https://doi.org/10.1039/c6cc06228h.
[11] C. Kang, S. Yang, M. Tan, C. Wei, Q. Liu, J. Fang, G. Liu, Purification of copper nanowires to prepare flexible transparent conductive films with high performance, ACS Appl. Nano Mater. 1 (2018) 3155–3163, https://doi.org/10.1021/acsanm.8b00326.
[12] A.S. Hashimi, R.T. Ginting, S.X. Chin, K.S. Lau, M.A. Nazhif Mohd Nohan, S. Zakaria, C.C. Yap, C.H. Chia, Fast microwave-assisted synthesis of copper nanowires as reusable high-performance transparent conductive electrode, Curr. Appl. Phys. 20 (2020) 205–211, https://doi.org/10.1016/j.cap.2019.11.006.
[13] Z. Yin, S. Chen, Y. Guan, Q. Ran, Q. Zhang, X. Yan, R. Jin, H. Yu, L. Li, J. Yu, Copper nanowire dispersion through an electrostatic dispersion mechanism for high-performance flexible transparent conducting films and optoelectronic devices, ACS Appl. Mater. Interfaces 11 (2019) 5264–5275, https://doi.org/10.1021/acsami.8b19277.
[14] C. Hwang, J. An, B.D. Choi, K. Kim, S.W. Jung, K.J. Baeg, M.G. Kim, K.M. Ok, J. Hong, Controlled aqueous synthesis of ultra-long copper nanowires for stretchable transparent conducting electrode, J. Mater. Chem. C Mater. 4 (2016) 1441–1447, https://doi.org/10.1039/c5tc03614c.
[15] Y. Zhang, J. Xia, Y. Liu, L. Qiang, L. Zhu, Impacts of morphology, natural organic matter, cations, and ionic strength on sulfidation of silver nanowires, Environ. Sci. Technol. 50 (2016) 13283–13290, https://doi.org/10.1021/acs.est.6b03034.
[16] J. Koo, S. Kwon, N.R. Kim, K. Shin, H.M. Lee, Ethylenediamine-enhanced oxidation resistivity of a copper surface during water-based copper nanowire synthesis, J. Phys. Chem. C 120 (2016) 3334–3340, https://doi.org/10.1021/acs.jpcc.5b10733.
[17] L. Gan, Y. Liu, X. Yang, J. Chen, N. Yang, Y. Zhu, Stability of silver nanowire transparent conductive film and strategies for improvement, Crit. Rev. Solid State Mater. Sci. 50 (2025) 1–53, https://doi.org/10.1080/10408436.2024.2379246.
[18] Z. Niu, F. Cui, Y. Yu, N. Becknell, Y. Sun, G. Khanarian, D. Kim, L. Dou, A. Dehestani, K. Schierle-Arndt, P. Yang, Ultrathin epitaxial Cu@Au core-shell nanowires for stable transparent conductors, J. Am. Chem. Soc. 139 (2017) 7348–7354, https://doi.org/10.1021/jacs.7b02884.
[19] A.R. Rathmell, S.M. Bergin, Y.L. Hua, Z.Y. Li, B.J. Wiley, The growth mechanism of copper nanowires and their properties in flexible, transparent conducting films, Adv. Mater. 22 (2010) 3558–3563, https://doi.org/10.1002/adma.201000775.
[20] Q. Xie, Z. Yan, S. Wang, Y. Wang, L. Mei, F. Qin, R. Jiang, Transparent, flexible, and stable polyethersulfone/copper-nanowires/polyethylene terephthalate sandwich-structured films for high-performance electromagnetic interference shielding, Adv. Eng. Mater 23 (2021), https://doi.org/10.1002/adem.202100283.
[21] J.M. Chiu, I. Wahdini, Y.N. Shen, C.Y. Tseng, J. Sharma, Y. Tai, Highly stable copper nanowire-based transparent conducting electrode utilizing polyimide as a protective layer, ACS Appl. Energy Mater 6 (2023) 5058–5066, https://doi.org/10.1021/acsaem.3c00703.
[22] S. Zhao, F. Han, J. Li, X. Meng, W. Huang, D. Cao, G. Zhang, R. Sun, C.P. Wong, Advancements in copper nanowires: synthesis, purification, assemblies, surface modification, and applications, Small 14 (2018), https://doi.org/10.1002/smll.201800047.
[23] X. Li, Y. Wang, C. Yin, Z. Yin, Copper nanowires in recent electronic applications: progress and perspectives, J. Mater. Chem. C Mater. 8 (2020) 849–872, https://doi.org/10.1039/c9tc04744a.
[24] Y. Zhang, J. Guo, D. Xu, Y. Sun, F. Yan, Synthesis of Ultralong copper nanowires for high-performance flexible transparent conductive electrodes: the effects of polyhydric alcohols, Langmuir 34 (2018) 3884–3893, https://doi.org/10.1021/acs.langmuir.8b00344.
[25] N.H. Tran, P. Tran, J.H. Lee, Copper nanowire-sealed titanium dioxide/poly (dimethylsiloxane) electrode with an In-plane wavy structure for a stretchable capacitive strain sensor, ACS Appl. Nano Mater. 5 (2022) 7150–7160, https://doi.org/10.1021/acsanm.2c00963.
[26] S. Yu, Z. Liu, L. Zhao, B. Gong, High-performance flexible transparent conductive tape based on copper nanowires, Opt. Mater. (Amst) (2021) 119, https://doi.org/10.1016/j.optmat.2021.111301.
[27] A. Barua, R. Gogoi, P.G. Reddy, S. Jolaiy, M. Bodaghi, T. Laukkanen, T. Speck, V. Sariola, V. Sharma, Biomimetic freestanding microfractals for flexible electronics, Npj Flex. Electron. 9 (2025) 10, https://doi.org/10.1038/s41528-025-00381-z.
[28] H. Xiang, T. Guo, M. Xu, H. Lu, S. Liu, G. Yu, Ultrathin copper nanowire synthesis with tunable morphology using organic amines for transparent conductors, ACS Appl. Nano Mater. 1 (2018) 3754–3759, https://doi.org/10.1021/acsanm.8b00722.
[29] Y. Shi, H. Li, L. Chen, X. Huang, Obtaining ultra-long copper nanowires via a hydrothermal process, Sci. Technol. Adv. Mater. 6 (2005) 761–765, https://doi.org/10.1016/j.stam.2005.06.008.
[30] Z. Yin, C. Lee, S. Cho, J. Yoo, Y. Piao, Y.S. Kim, Facile synthesis of oxidation-resistant copper nanowires toward solution-processable, flexible, foldable, and free-standing electrodes, Small 10 (2014) 5047–5052, https://doi.org/10.1002/smll.201401276.
[31] P. Scherrer, Estimation of the size and internal structure of colloidal particles by means of Röntgen. Nachrichten von der Gesellschaft der Wissenschaften zu Göttingen, Nachrichten von Der Gesellschaft der Wissenschaften Zu Göttingen, Math.-Phys. Kl. 2 (1918) 98–100.
[32] P. Bellchambers, M. Walker, S. Huband, A. Dirvanauskas, R.A. Hatton, Enhanced oxidation stability of transparent copper films using a hybrid organic-inorganic nucleation layer, ChemNanoMat 5 (2019) 619–624, https://doi.org/10.1002/cnma.201800667.
[33] X. Zha, D. Gong, W. Chen, L. Wu, C. Zhang, Synthesis of copper nanowires using monoethanolamine and the application in transparent conductive films, Nanomaterials 15 (2025), https://doi.org/10.3390/nano15090638.
[34] M.C. Biesinger, L.W.M. Lau, A.R. Gerson, R.S.C. Smart, Resolving surface chemical states in XPS analysis of first row transition metals, oxides and hydroxides: sc, Ti, V, Cu and Zn, Appl. Surf. Sci. 257 (2010) 887–898, https://doi.org/10.1016/j.apsusc.2010.07.086.
[35] S. Hemmati, D.P. Barkley, Parametric study, sensitivity analysis, and optimization of polyol synthesis of silver nanowires, ECS J. Solid State Sci. Technol. (2017) 132.
[36] A.K. Kar, R. Srivastava, Selective synthesis of Cu-Cu 2 O/C and CuO-Cu 2 O/C catalysts for Pd-free C-C, C-N coupling and oxidation reactions, Inorg. Chem. Front. 6 (2019) 576–589, https://doi.org/10.1039/c8qi01198b.
[37] F. Basarir, S. De, H. Daghigh Shirazi, J. Vapaavuori, Ultra-long silver nanowires prepared via hydrothermal synthesis enable efficient transparent heaters, Nanoscale Adv. (2022), https://doi.org/10.1039/d2na00560c.
[38] S. Mourdikoudis, M. Menelaou, N. Fiuza-Maneiro, G. Zheng, S. Wei, J. Pérez-Juste, L. Polavarapu, Z. Sofer, Oleic acid/oleylamine ligand pair: a versatile combination in the synthesis of colloidal nanoparticles, Nanoscale Horiz. 7 (2022) 941–1015, https://doi.org/10.1039/d2nh00111j.
[39] J. Zhang, X. Zhu, J. Xu, R. Xu, H. Yang, C. Kan, Comparative study on preparation methods for transparent conductive films based on silver nanowires, Molecules 27 (2022), https://doi.org/10.3390/molecules27248907.
[40] R. Wang, H. Ruan, Synthesis of copper nanowires and its application to flexible transparent electrode, J. Alloys Compd. 656 (2016) 936–943, https://doi.org/10.1016/j.jallcom.2015.09.279.
[41] M. Suchodol, H. Vejayan, X. Zhou, B. Jiang, H. Guo, R.D. Beck, Probing water dissociation and oxygen replacement on partially oxygen-covered Cu(111) by reflection absorption infrared spectroscopy, J. Phys. Chem. Lett. 14 (2023) 7848–7853, https://doi.org/10.1021/acs.jpclett.3c02004.
[42] D. Kim, J. Kwon, J. Jung, K. Kim, H. Lee, J. Yeo, S. Hong, S. Han, S.H. Ko, A transparent and flexible capacitive-force touch pad from high-aspect-ratio copper nanowires with enhanced oxidation resistance for applications in wearable electronics, Small Methods 2 (2018), https://doi.org/10.1002/smtd.201800077.

[43] J.J. Patil, W.H. Chae, A. Trebach, K.J. Carter, E. Lee, T. Sannicolo, J.C. Grossman, Failing forward: stability of transparent electrodes based on metal Nanowire networks, Adv. Mater. 33 (2021), https://doi.org/10.1002/adma.202004356.
[44] S. Nilsson, J.N. El Berch, D. Albinsson, J. Fritzsche, G. Mpourmpakis, C. Langhammer, The role of grain boundary sites for the oxidation of copper catalysts during the CO oxidation reaction, ACS Nano 17 (2023) 20284–20298, https://doi.org/10.1021/acsnano.3c06282.
[45] B. Maack, N. Nilius, Impact of granularity on the oxidation kinetics of copper, Phys. Status Solidi B Basic Res. 257 (2020), https://doi.org/10.1002/pssb.201900778.
[46] B. Zhang, Z. Zhou, J. Huang, J. Zhan, Q. Yao, R. Lu, R. Hu, B. Zhu, Interfacial engineering of nano-copper: mechanisms, strategies, and innovations for oxidation resistance, Nanoscale Adv. 7 (2025) 7109–7127, https://doi.org/10.1039/d5na00716j.
[47] S.-S. Yeh, W.-Y. Chang, J.-J. Lin, Probing nanocrystalline grain dynamics in nanodevices. https://www.science.org, 2017.
[48] P. Jaita, K. Saenkam, G. Rujijanagul, Improvements in piezoelectric and energy harvesting properties with a slight change in depolarization temperature in modified BNKT ceramics by a simple technique, RSC Adv. 13 (2023) 3743–3758, https://doi.org/10.1039/d2ra07587c.
[49] A. Asthana, K. Momeni, A. Prasad, Y.K. Yap, R.S. Yassar, In situ observation of size-scale effects on the mechanical properties of ZnO nanowires, Nanotechnology 22 (2011), https://doi.org/10.1088/0957-4484/22/26/265712.
[50] H.C. Chu, Y.C. Chang, Y. Lin, S.H. Chang, W.C. Chang, G.A. Li, H.Y. Tuan, Spray-deposited large-area copper nanowire transparent conductive electrodes and their uses for touch screen applications, ACS Appl. Mater. Interfaces 8 (2016) 13009–13017, https://doi.org/10.1021/acsami.6b02652.
[51] B. Sharma, R.M. Singh, A. Kumar, S. Kumar, Diameter-dependent properties of electrodeposited nickel nanowire arrays, J. Mater. Sci.: Mater. Electron. 33 (2022) 14323–14333, https://doi.org/10.1007/s10854-022-08358-8.
[52] K. Critchley, B.P. Khanal, M.L. Górzny, L. Vigderman, S.D. Evans, E.R. Zubarev, N. A. Kotov, Near-bulk conductivity of gold nanowires as nanoscale interconnects and the role of atomically smooth interface, Adv. Mater. 22 (2010) 2338–2342, https://doi.org/10.1002/adma.201000236.
[53] A.J. Cheng, L. Wu, Z. Sha, W. Chang, D. Chu, C.H. Wang, S. Peng, Recent advances of capacitive sensors: materials, microstructure designs, applications, and opportunities, Adv. Mater. Technol. 8 (2023), https://doi.org/10.1002/admt.202201959.
[54] D.J. Griffiths, Introduction to Electrodynamics, 5th ed, Cambridge University Press, 2024.
[55] Z. Yu, X. Jian, J. Wang, X. Zhang, S. Zhai, Advantages and research progress of polycarbonates in flexible electronic devices, Macromol, Rapid Commun. (2025), https://doi.org/10.1002/marc.202500705.